Modelling of autogenous healing in Ultra High Performance Concrete

Benoit Hilloulin, Frederic Grondin, M. Matallah, Ahmed Loukili

Modelling of autogenous healing in Ultra High Performance Concrete

B. Hilloulin [1], F. Grondin [1], M. Matallah [2, 1] and A. Loukili [1]

[1] *LUNAM Université, Institut de Recherche en Génie Civil et Mécanique (GeM), UMR-CNRS 6183, Ecole Centrale de Nantes, 1 rue de la Noë, 44321 Nantes, France – e-mail:* benoit.hilloulin@ec-nantes.fr; frederic.grondin@ec-nantes.fr; ahmed.loukili@ec-nantes.fr

[2] *RISAM (RISk Assessment & Management), Université de Tlemcen, BP230, Algérie – e-mail:* matallah@mail.univ-tlemcen.dz

Highlights

- A hydro-chemo-mechanical model of autogenous healing of concrete is developed.
- Mechanical properties of the healed crack are assessed.
- Quantification of the healing product mechanical properties is proposed.

Abstract

The restoration of ultra high performance concrete (UHPC) specimens due to the self-healing phenomenon was investigated in this paper. A hydro-chemo-mechanical model based on micro-mechanical observations was established. The aim was to evaluate the mechanical properties of the new healing products in order to describe the partial recovery of the mechanical properties of healed concrete. An analysis of the influence of some physical parameters provided first explanations about the self-healing phenomenon. It was shown that the mechanical properties of CSH in the healed crack are lower than the ones of the virgin material.

Keywords: Self-healing (C), Modelling (E), Mechanical properties (C), Calcium-Silicate-Hydrate (C-S-H) (B), Characterization (B)

1. Introduction

Although occurrence of cracks in concrete structures is taken into consideration during design, cracks generate important inspection and repairing costs. Some of them can seriously affect the durability and the stability of the structures. Thus, self-healing concrete could be a mean to make important savings decreasing direct and indirect costs caused by repairing works [1, 2]. It has been observed by many researchers that cracks in concrete can heal naturally, without any particular additive, under favourable conditions [3-11]. This phenomenon called 'autogenous' healing is the consequence of two main reactions [12]: further hydration of unhydrated particles upon water ingress into the crack, especially for concrete with an important amount of unhydrated cement particles [13, 14] and precipitation of calcium carbonate due to the reaction between calcium contained in the cementitious matrix with carbon dioxide dissolved in the water filling the crack [15]. Some studies have reported the predominance of the precipitation phenomenon in common concrete with a water-to-cement (w/c) ratio around 0.5 leading to the filling of cracks with an initial width up to around 200 µm [10]. Autogenous healing by further hydration has been studied by several researchers because of expected mechanical regains due to the creation of new calcium silicate hydrates (C-S-H). A global recovery of stiffness can be achieved by further hydration [16, 18]. But, regains in compressive or flexural strengths have been found to be limited [8, 10, 14] because of relatively poor mechanical properties of the healing product.

Only few models were developed to describe self-healing of concrete. Some models were proposed to determine the amount of unhydrated cement particles in concrete specimens considering w/c ratio and cement fineness which underlies the self-healing potential [17, 19, 20], or to calculate the amount of healing product due to further hydration considering two crack modes [21, 22]. Recently, Huang and Ye [23, 24] developed a model simulating

further hydration by water release by a capsule in a crack using water transport theory, ion diffusion theory and thermodynamics theory. However, these models do not provide any information about the mechanical effects of self-healing.

In this study, a hydro-chemo-mechanical model was developed to simulate autogenous healing by further hydration with the aim to explain the mechanical regains after healing and provide information about the self-healing product. Experimentally, Granger et al. [14] used ultra high performance cementitious material (UHPC) with a w/c ratio close to 0.2 to study the self-healing of small cracks with initials widths of 10, 20 and 30 µm. Mechanical properties of healed and uncracked specimens were compared at different stages (1 week, 3 weeks, 10 weeks, 20 weeks and 40 weeks). The hydro-chemo-mechanical model has been implemented in the finite element code Cast3M [25] to calculate the self-healing potential of a damaged concrete beam after cracking using three-point-bending test. Damage has been calculated by a modified microplane model [26, 27]. Ingress of water has been simulated by the Fick's law and water interaction with the unhydrated cement particles led to their hydration considering a hydration model [28, 29]. The recovery of mechanical properties of the cracked concrete beam was obtained by decreasing the local damage value due to the filling of empty spaces by new hydrates. In the first part of this article, the relationships underlying the model will be explained into details and the model algorithm will be presented. Furthermore, the numerical results will be compared with experimental measurements and an analysis of the self-healing phenomenon will be suggested.

2. Description of the self-healing model

2.1. Problem formulation

The resolution of the global problem consists on the resolution of a first mechanical problem (P1) corresponding to the initial creation of a single crack, followed by a coupled hydro-chemical problem corresponding to the healing process (P2), and is concluded by a second resolution of a mechanical problem (P3) due to the mechanical changes implicated by the healing process.

We consider a volume V representing the specimen. The specimen is submitted to successive loads of different types: displacements $\overline{U}_i$ are applied on the boundaries Γ_i^u, the force $\overline{F}$ is applied on the boundary Γ^σ, the velocity (or pressure, or concentration) is applied on the boundary Γ^C. The problems P1 and P3 are similar and lead to the calculation of the local displacement fields ($\underline{u}(\underline{y})$), strain fields ($\underline{\underline{\varepsilon}}(\underline{y})$) and stress fields ($\underline{\underline{\sigma}}(\underline{y})$) as follow (where volume forces are negligible):

$$\underline{div}\,\underline{\underline{\sigma}} = \underline{0} \qquad \underline{y} \in V \qquad (1)$$

$$\underline{\underline{\sigma}}(\underline{y}) = (1 - d(\underline{y}))\,\widetilde{C}^t(\underline{y}) : (\underline{\underline{\varepsilon}}(\underline{y}) - \underline{\underline{\varepsilon}}^p(\underline{y})) \qquad \underline{y} \in V \qquad (2)$$

$$\underline{\underline{\varepsilon}}(\underline{y}) = \frac{1}{2}\left(\underline{\underline{\nabla}}\,\underline{u}(\underline{y}) + {}^t\,\underline{\underline{\nabla}}\,\underline{u}(\underline{y})\right) \qquad \underline{y} \in V \qquad (3)$$

$$\underline{u}(\underline{y}) = \overline{U}_i \qquad \underline{y} \in \Gamma_i^u \qquad (4)$$

$$\overline{F} = \underline{\underline{\sigma}}(\underline{y}).\underline{n} \qquad \underline{y} \in \Gamma^\sigma \qquad (5)$$

where $\widetilde{C}^t(\underline{y})$ represents the local stiffness tensor of 4th order depending on the time (t = 0 corresponds to the problem P1, and t > 0 corresponds to the problem P3) and $\underline{\underline{\varepsilon}}^p$ the

plastic strain (computed using a loading function by the normality rule). The evolution of the damage is given by [27]:

$$d = 1 - \frac{\varepsilon_{d0}}{\varepsilon_{eq}} \exp\left[B_t\left(\varepsilon_{d0} - \varepsilon_{eq}\right)\right] \quad (6)$$

where $B_t = \dfrac{f_t}{\dfrac{G_f}{h} - \dfrac{f_t \cdot \varepsilon_{d_0}}{2}}$ represents a damage parameter to control the slope of the strain softening constitutive relation in function of the width *h* of the finite element and the fracture energy [36], $\varepsilon_{d0} = \dfrac{f_t}{E}$ the strain threshold and ε_{eq} the equivalent strain ($\varepsilon_{eq} = \sqrt{\overline{\overline{\varepsilon}^{e}} : \overline{\overline{\varepsilon}^{e}}}$ where $\overline{\overline{\varepsilon}^{e}}$ is the elastic strain).

To model the autogenous self-healing (problem P2), external humidity conditions are considered by the contact with water on the boundary of the beam (initial concentration of water of 1 outside the beam, 0.2 inside the beam). The ingress of water, with a speed U, through the damaged material was simulated by using the Fick's law:

$$\frac{\partial U}{\partial T} = D(d)\frac{\partial^2 U}{\partial X^2} \quad (7)$$

where D(d) represents the diffusion coefficient depending on damage [30, 31]. The evolution of the diffusivity coefficient is calibrated to follow the evolution of the permeability coefficient with damage (eq 8) [31, 32]. For small damage values, it corresponds to an exponential law and for damage values close to 1, it fits the Poiseuille's law. The evolution of the diffusivity coefficient D(d) is presented in Figure 1.

$$\log(k) = (1-d)\log(k_p) + d\log(k_d) \quad (8)$$

Where $k_p = u^2/12$ is the permeability for damage close to 1 (u is the crack opening) and $k_d = k_0 \exp((\alpha D)^{\beta})$ is the permeability for small damage values between 0 and 0.15 (k0

is the initial permeability, α and β two constants ranging respectively from 9.4 to 12.3 and 1.4 to 1.6) [30].

The local quantity of water inside the beam is then used to activate the hydration process which determines the volume of each component in the microstructure according to Arrhenius' equation [28, 29]:

$$\tau_i \frac{d\xi_i}{dt} = \tilde{A}(\xi_i) \tag{9}$$

where $\tilde{A}$ and τ represent the normalized affinity and the characteristic time, respectively, ξ_i the hydration coefficient of the clinker i.

The hydration process leads to the dissolution of clinkers and to the formation of hydrates with a volume defined by:

$$V_k^P(t) = \sum_l^n \left(V_i^0 \frac{n_k^P M_k}{n_l^R M_l} \frac{\rho_C}{\rho_k} \right) \xi_l(t) \qquad k = 1, m \tag{10}$$

where V_i^0 represents the residual clinkers in concrete, V_k^P the new formed hydrates, M the molar mass, ρ the mass density and n the mole. The index *k* represents the products (clinkers), *l* the reactants and *c* the cement.

According to the definition of damage as a void volume in the material, we suppose that when the hydration products are created in the damage area, they fill the empty space and decrease the local damage value:

$$d_{final} = d_{initial} - k \frac{V_{hydrates}}{V_{total}} \tag{11}$$

Where k is a coefficient to eventually adjust the final damage value after healing due to the healing potential, a value of 1 is considered in this study. Up to now, the contribution

136 of a given healing product from autogenous healing to the observed regain in mechanical
137 properties is not evident. In the experimental results reported here, almost no calcite was
138 formed, so the coefficient k should be higher than for other concrete were the healing
139 product is a mix of CSH, portlandite and calcite. One should adjust the coefficient k to
140 the effective amount of CSH product created by further hydration.
141 The decrease of the local damage value leads to a decrease of the quantity of water
142 absorbed into the crack during the following time step due to the decrease of the diffusion
143 coefficient.
144 A condensed flowchart of the model is presented in Figure 2.
145

146 **2.2. Modelling system**

147 Finite element analysis were performed on a UHPC notched beam (50 cm x 10 cm x
148 5 cm) with a notch depth of 2 cm as used by Granger et al. [14]. The centre part of the
149 beam was discretized with elements of 0.75 mm x 1 mm size. Three-point-bending tests
150 were simulated on a concrete beam before and after healing to simulate, respectively, the
151 creation of a single crack, and the restoration of the mechanical properties.
152 The numerical simulations have been performed under displacement control with
153 constant displacement step of $5x10^{-7}$ m at the top of the beam, considering a vertical
154 displacement of the notch where the load was applied and rolling supports under the beam
155 as illustrated in Figure 3. The crack mouth opening displacement (CMOD) was calculated
156 considering the evolution of the relative displacement of two nodes placed under the
157 beam, at the same position as in the experimental instrument (1 cm of initial opening).
158 For the healing procedure, an initial moisture diffusion coefficient of 10^{-9} m²/s was
159 considered for undamaged zones [33].

In order to describe the hydration process at a mesoscopic scale, an initial uniform volume fraction of clinker of 0.12 was applied. This initial volume fraction corresponds to a volume fraction of anhydrous clinkers of around 50% in the cement paste. The local volume fraction of clinker was decreased at each time step after the diffusion of water according the pre-set hydration speed. The first hydration speed considered in this study was comparable to a speed of a new concrete mix. The hydration speed was then decreased to investigate its role on the healing kinetics.

Different numerical time steps were investigated from 1 second to 6 hours after several days of healing.

3. Results and discussion

3.1. Pre-cracking stage and mechanical parameters of the virgin specimen

Some constitutive damage parameters (Young's modulus (E), Poisson's ratio (ν), tensile and compressive strengths (f_t and f_c)) were measured experimentally and fracture energy (G_f) was adjusted to perform the three-point-bending simulations on a notched beam, in order to fit the experimental loading curves during the stage of the creation of the crack. The selected parameters for the mechanical model are presented in Table 1. These parameters gave correct initial stiffness and maximal bearing load and also led to a correct agreement concerning the unloading slope and the final CMOD (around 10 µm) as illustrated in Figure 4. The latter are important in scope to fairly compare numerical and experimental reloading results.

3.2. Healing

3.2.1. Influence of the healing parameters on the extend of the healed zone

184 Healing is located all along the crack if the evolution of the diffusion coefficient with
185 damage is the one previously presented. Indeed, diffusion through the crack only takes
186 tens of seconds while the hydration process duration is of around some hours. If the speed
187 of hydration is increased (which seems to be a relevant hypothesis because the high water
188 content in the crack [24] and the direct exposure of clinker on the crack surface), damage
189 can decreased faster locally. Then, the healed zone is located at the bottom part of the
190 crack (Figure 5) because the local reduction of the damage slows down the diffusion
191 process. Thus, the healed zone grows slowly to the top of the beam.
192 Experimentally, healing products (mainly C-S-H) are generally observed all along the
193 crack [14, 34]. The model can reproduce this trend even though it existed risk of the
194 partial filling of the crack due to its small width. However, this first model considering
195 the water diffusion and the hydration of anhydrous clinker is rather sensitive to the input
196 parameters (speed of rehydration and speed of diffusion as illustrated in Figure 5). Due
197 to the dependence of the model on the speed of rehydration, the choice has been made to
198 develop an external procedure to localise the healing product to focus on the mechanical
199 part of the model in order to identify material parameters of the healing product.

200 **3.2.2. External localisation procedure and two-phase healing model**

201 In order to limit the dependence of the results on the speed on hydration of clinkers, an
202 external procedure (independent of the hydro-chemical procedure) was developed to
203 localise the healed zone considering the initial crack width and study its influence without
204 taking into consideration the diffusion process described earlier. This procedure was
205 developed to easily study the influence of the size of healed zone on the mechanical
206 regains. Considering that it was not possible to input variably distributed mechanical
207 properties in this external procedure (to represent the evolution of the filling fraction for
208 example), mechanical parameters corresponding to the healing product were input in the

bottom part of the beam, where the water can react directly with the clinker and fill the crack very quickly. For larger cracks, it is possible that the majority of the healing products could be located where the local crack width would be reasonable (< 100 - 200 microns [10]).

Numerical calculation of the initial crack width was performed according to OUVFISS procedure implemented in Cast3M [35]. Figure 6 a) represents the initial numerical crack width. The initial crack width calculated with this procedure is 8.6 µm. It consists well with the measured CMOD around 10 .

A two-phase healing model, illustrated in Figure 6 b), was then developed to study the influence of the mechanical parameters of the healing product on the global mechanical behaviour. The bottom part of the crack, corresponding to the zone where the crack width was larger than the width input in the localisation procedure, was modelled with mechanical parameters independent of the parameters of the virgin specimen. This zone (Z1) situated in the bottom part of the crack is supposed to model the C-S-H healing product. Other mechanical parameters were attributed to the upper part of the crack. This zone (Z2) is supposed to model the mechanical properties of all the others entities present in the crack except the C-S-H healing product. Although the model does not take into account the experimental localisation of the healing product all along the crack, it allows representing the gradient of properties existing in the crack.

3.3. Reloading

3.3.1. Influence of the extend of the healed zone

Because the main interest of the hydro-chemical procedure is the localisation of the healed zone, the influence of this localisation on the mechanical properties of the healed specimen was firstly studied. Several reloading with different healed zone sizes and

234 localisations were simulated assuming the same mechanical properties for the healing
235 product than for the virgin specimen (damage locally reduced to 0).
236 When the bottom part of the crack was not healed, the initial slope of the reloading curve
237 in the load vs CMOD graph was smaller than all the experimental results with healing.
238 This could indicate that healing products were formed at the bottom part of the crack even
239 if it was the wider part of the crack. It could be explained by the small maximum aperture
240 of the crack which is comparable to the size of the unhydrated clinker and therefore more
241 likely to be closed by hydration products. The healing localisation may be different for
242 wider cracks with maximum crack width of around 100-300 µm because hydration
243 products (C-S-H) cannot fill this gap completely as reported by many experimental
244 studies [10, 15, 17].
245 On the other hand, healing in the bottom part of the crack is not sufficient to restore the
246 mechanical properties (stiffness and maximum bearing load) even if the healing product
247 has the same mechanical properties as the virgin specimen. Extend of the healed zone
248 needs to be sufficient. In our model, a height of the healed zone of around one fourth of
249 the crack length (zone where the initial crack width is larger than 7 µm) seems sufficient
250 to restore the initial slope of the load vs. CMOD curve and also the maximum bearing
251 load as illustrated in Figure 7. If the healed zone is too small (zone where the initial crack
252 width is larger than 8-8.5 µm which leads to a length of the healed zone of around one
253 eighth to one tenth of the initial crack length) the maximum bearing load and the stiffness
254 cannot consist well with experimental results. In this case, the maximum bearing load
255 increases with the size of the healed zone.
256 Thus, according to the experimental results showing a rather quick regain in stiffness
257 (different than the hysteresis phenomenon) and the numerical calculations, we can assume

that healing product was, at least, created at the bottom part of the crack and likely recover an extended part of the crack.

3.3.2. Influence of the mechanical parameters of the healing product

As exemplified by Figure 7, the experimental bi-linear shape of the reloading curve cannot be reproduced assuming that the healing product has the same mechanical properties than the virgin specimen. Consequently, new mechanical parameters were input to describe the healing product with the two-phase healing model. Thus, it is possible to simulate a healing product with heterogeneous mechanical properties.

According to the two-phase healing model, the bi-linear shape of the experimental reloading curves can mainly be attributed to the difference of the Young's modulus in the two different phases. This difference between the two numerical Young's modulus highlights the heterogeneity of the healed crack: some zones are healed with healing products with very good mechanical properties whereas other zones have very poor mechanical properties because they remain fractured.

The maximum bearing load obtained with the simulation is mainly influenced by the fracture energies assigned to both zones. Thus, the small experimental regain in bearing load could be explained by a lower fracture energy in the crack than in the undamaged zone. It leads to an easier recreation and propagation of a crack through the healed zone which has been reported in the experimental observation.

3.3.3. Comparison between numerical and experimental curves and evolution of the healing product properties

Numerical simulations were performed adjusting the height of the Zone 1 and the mechanical parameters of both zones in order to fit the experimental curves and obtain

283 information about the evolution of the healing product over time. The best fitting curves
284 were selected in order to reproduce the original stiffness and the maximum bearing load.
285 These numerical curves were obtained with the parameters detailed in Table 2 and are
286 presented in Figure 8. On all the numerical curves, we can notice an overestimation of
287 the load corresponding to the end of the first initial slope followed by a small drop in
288 load. This is due to the two-phase model where the mechanical properties are not
289 continuous between the two phases. Regarding the material stiffness for the 'No healing'
290 case, numerical and experimental results cannot be compared. Although the mechanical
291 model implemented here reproduce realistic decrease of stiffness and CMOD, it does not
292 reproduce the hysteretic behaviour creating the small recover in stiffness for the cracked
293 specimens due to friction between cracks lips.
294 The size of Z1 was increased with the healing time. This could indicate that, even if the
295 hydration of the first clinker is very quick (first healing products are created within some
296 hours), healing product is still created after some weeks in water. Thus, self-healing by
297 further hydration could follow a 'surface controlled - diffusion controlled process' as
298 described for the precipitation of calcite [15].
299 The mechanical properties inputted the two zones are different than the ones of the virgin
300 specimen. Young's modulus and fracture energy in Z1 are higher than the ones in the
301 virgin specimen. This could be explained by the better mechanical properties of pure C-
302 S-H compared to the concrete. Also, we can notice that the fracture energy of Z1 increases
303 with time [36] which indicates that the healing product has a higher resistance to crack
304 propagation as the healing phenomenon progress. The mechanical properties affected to
305 Z2 are very low and consist well with the ones of an almost completely damaged zone
306 (Young's modulus close to 0).
307

4. Conclusions

In this study, a hydro-chemo-mechanical model for self-healing concrete was developed. The localisation of the healed zone was investigated based on a diffusion-hydration model. Regains in mechanical properties due to healing were assessed with a continuum damage model. Based on the experiments and simulations, conclusions can be drawn as follows:

- The mechanical properties of the healed crack are lower than the ones of the virgin material at a mesoscopic scale. This is explained by the partial healing along the crack which leads to a relatively small regain in bearing capacity after healing.
- The evolution of the mechanical properties of the healing product (Young's modulus, fracture energy) with time and the increase of its quantity over time explain the evolution of the mechanical properties of the concrete structure.
- Partial healing of cracks located around the zone in contact with water can be explained by the decrease of water flow with time due to the formation of healing products. The speed of formation of new hydrates in small cracks could be higher than the speed of the original hydration (with possibly no induction period).
- A relatively small healed zone with mechanical properties close to the virgin mechanical properties can lead to substantial regain in the structure mechanical properties (in autonomous healing solutions for example).

Modelling the autogenous healing in concrete is still a great challenge because it relies on the development of coupled models. Further investigations are needed to understand the recovery of mechanical and transport properties. In the future, numerical models may help to assist experimental observations and participate to predict the evolution of concrete structures properties during their service life.

Acknowledgements

Financial support from the GIS LIRGeC, Région Pays de la Loire (France), for this study is gratefully acknowledged.

References

[1] K. van Breugel, Self-healing concepts in civil engineering for sustainable solutions: Potential and constraints, in: Proceedings of the Second International Conference on Self-Healing Materials, 2009.

[2] M. de Rooij, K. Van Tittelboom, N. De Belie, E. Schlangen (Eds), Self-Healing Phenomena in Cement-Based Materials, Springer Netherlands, 2013.

[3] C. A. Clear, The effect of autogenous healing upon leakage of water through cracks in concrete, Cement and Concrete Association (1985).

[4] N. Hearn, C. Morley, Self-sealing property of concrete - experimental evidence, Materials and Structures 30 (7) (1997) 404–411

[5] H.-W. Reinhardt, M. Jooss, Permeability and self-healing of cracked concrete as a function of temperature and crack width, Cement and Concrete Research 33 (7) (2003) 981 – 985.

[6] M. Li, V. C. Li, Cracking and healing of engineered cementitious composites under chloride environment, ACI Materials Journal 108 (2011) 333–340.

[7] S. Jacobsen, J. Marchand, L. Boisvert, Effect of cracking and healing on chloride transport in OPC concrete, Cement and Concrete Research 26 (6) (1996) 869 – 881.

[8] S. Jacobsen, E. J. Sellevold, Self healing of high strength concrete after deterioration by freeze/thaw, Cement and Concrete Research 26 (1) (1996) 55 – 62.

[9] Y. Yang, M. D. Lepech, E.-H. Yang, V. C. Li, Autogenous healing of engineered cementitious composites under wet-dry cycles, Cement and Concrete Research 39 (5) (2009) 382 – 390.

[10] K. Van Tittelboom, E. Gruyaert, H. Rahier, N. De Belie, Influence of mix composition on the extent of autogenous crack healing by continued hydration or calcium carbonate formation, Construction and Building Materials 37 (0) (2012) 349 – 359.

[11] S. Jacobsen, J. Marchand, H. Hornain, Sem observations of the microstructure of frost deteriorated and self-healed concretes, Cement and Concrete Research 25 (8) (1995) 1781 – 1790.

[12] A. Neville, Autogenous healing: A concrete miracle?, Concrete international 24 (2002) 76–81.

[13] Y. Abdel-Jawad, F. Dehn, Self-healing of self-compacting concrete, in: Fourth International RILEM Symposium on Self-Compacting Concrete (SCC 2005), 2005, pp. 1023–1029.

[14] S. Granger, A. Loukili, G. Pijaudier-Cabot, G. Chanvillard, Experimental characterization of the self-healing of cracks in an ultra high performance cementitious material: Mechanical tests and acoustic emission analysis, Cement and Concrete Research 37 (4) (2007) 519 – 527.

[15] C. Edvardsen, Water permeability and autogenous healing of cracks in concrete, ACI Materials Journal 96 (4) (1999) 448–454.

[16] P. Pimienta, G. Chanvillard, Durability of UHPFRC specimens kept in various aggressive environments, in: Proceedings of the 10th International Conference On Durability of Building Materials and Components LYON [France] 17-20 April 2005.

[17] N. Ter Heide, Crack healing in hydrating concrete, Master's thesis, Delft University of Technology (2005).

[18] N. Ter Heide, E. Schlangen, Self healing of early age cracks in concrete, in: Proceedings of the First international conference on Self Healing Materials, Noordwijk aan Zee, The Netherlands, 18-20 April 2007.

[19] H. He, Z.-Q. Guo, P. Stroeven, M. Stroeven, L. Sluys, Self-healing capacity of concrete - computer simulation study of unhydrated cement structure, Image Analysis & Stereology 26 (2007) 137–143.

[20] H. He, Z. Guo, P. Stroeven, M. Stroeven, Numerical assessment of concrete's self-healing potential for promoting durability, International Journal of Modelling, Identification and Control 7 (2009) 142–147.

[21] Z. Lv, H. Chen, Modeling of self-healing efficiency for cracks due to unhydrated cement nuclei in hardened cement paste, Procedia Engineering 27 (0) (2012) 281 – 290.

[22] Z. Lv, H. Chen, Self-healing efficiency of unhydrated cement nuclei for dome-like crack mode in cementitious materials, Materials and Structures (2013) 1–12.

[23] H. Huang, G. Ye, Simulation of self-healing by further hydration in cementitious materials, Cement and Concrete Composites 34 (4) (2012) 460 – 467.

[24] H. Huang, G. Ye, D. Damidot, Characterization and quantification of self-healing behaviors of microcracks due to further hydration in cement paste, Cement and Concrete Research 52 (0) (2013) 71 – 81.

[25] P. Verpaux, T. Charras, A. Millard, Castem 2000: une approche moderne du calcul des structures, Calcul des structures et intelligence artificielle (J.M. Fouet and P. Ladevèze and R. Ohayon) (1988) 261–271.

[26] S. Fichant, Endommagement et anisotropie induite du béton de structures. modélisations approchées, Ph.D. thesis, Ecole Normale Supérieure de Cachan (1996).

404 [27] S. Fichant, C. La Borderie, G. Pijaudier-Cabot, Isotropic and anisotropic
405 descriptions of damage in concrete structures, Mechanics of Cohesive-frictional Materials
406 4 (4) (1999) 339–359.
407 [28] O. Bernard, F.-J. Ulm, E. Lemarchand, A multiscale micromechanics-hydration
408 model for the early-age elastic properties of cement-based materials, Cement and
409 Concrete Research 33 (9) (2003) 1293 – 1309.
410 [29] F. Grondin, M. Bouasker, P. Mounanga, A. Khelidj, A. Perronnet, Physico-
411 chemical deformations of solidifying cementitious systems: multiscale modelling,
412 Materials and Structures 43 (1-2) (2010) 151–165.
413 [30] V. Picandet, A. Khelidj, G. Bastian, Effect of axial compressive damage on gas
414 permeability of ordinary and high-performance concrete, Cement and Concrete Research
415 31 (11) (2001) 1525 – 1532.
416 [31] A. Khelidj, M. Choinska, G. Chatzigeorgiou, G. Pijaudier-Cabot, Coupling
417 between progressive damage, temperature and permeability of concrete : experimental
418 and numerical study., Restoration of Buildings and Monuments 12 (2006) 299–316.
419 [32] M. Choinska, Effets de la température, du chargement mécanique et de leurs
420 intéractions sur la perméabilité du béton de structure, Ph.D. thesis, Ecole Centrale de
421 Nantes et Université de Nantes (2006).
422 [33] V. Picandet, G. Bastian, A. Khelidj, Compared imbibitions of ordinary and high
423 performance concrete with null or positive water pressure head, Cement and Concrete
424 Research 38 (6) (2008) 772 – 782.
425 [34] S. Granger, Caractérisation expérimentale et modélisation du phénoméne d'auto-
426 cicatrisation des fissures dans les bétons, Ph.D. thesis, Ecole Centrale de Nantes (2006).

427 [35] M. Matallah, C. La Borderie, O. Maurel, A practical method to estimate crack
428 openings in concrete structures, International Journal for Numerical and Analytical
429 Methods in Geomechanics 34 (15) (2010) 1615–1633.
430 [36] M. Matallah, M. Farah, F. Grondin, A. Loukili, E. Rozière, Size-independent
431 fracture energy of concrete at very early ages by inverse analysis, Engineering Fracture
432 Mechanics 109 (0) (2013) 1 – 16.
433

Table 1. Input mechanical parameters for the virgin specimen

$E^{(*)}$	$\nu^{(*)}$	f_t	$f_c^{(*)}$	G_f
45 GPa	0.2	7 MPa	90 MPa	50 N/m

$^{(*)}$ From experimental measurements

Table 2. Mechanical parameters input in the two-phase healing model

Simulation	Sim 1 week	Sim 10 weeks	Sim 20 weeks
Crack width separation Zone1/Zone2 (μm)	8	7.5	7
E_1 (GPa)	60	60	60
F_{t1} (MPa)	7.2	7.2	7.2
G_{f1} (N/m)	50	60	80
E_2 (GPa)	15	15	20
F_{t2} (MPa)	7.2	7.2	7.2
G_{f2} (N/m)	20	20	25

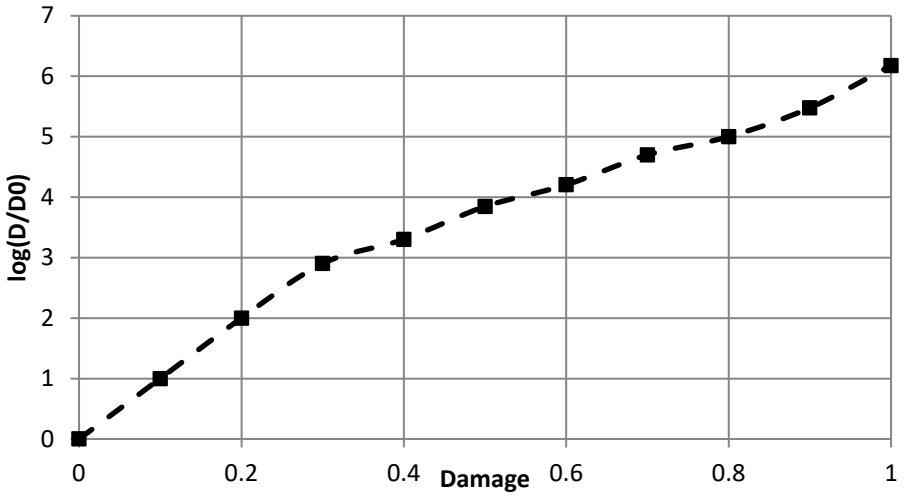

444

445 **Figure 1.** Evolution of the diffusivity coefficient with local damage

446

447

448

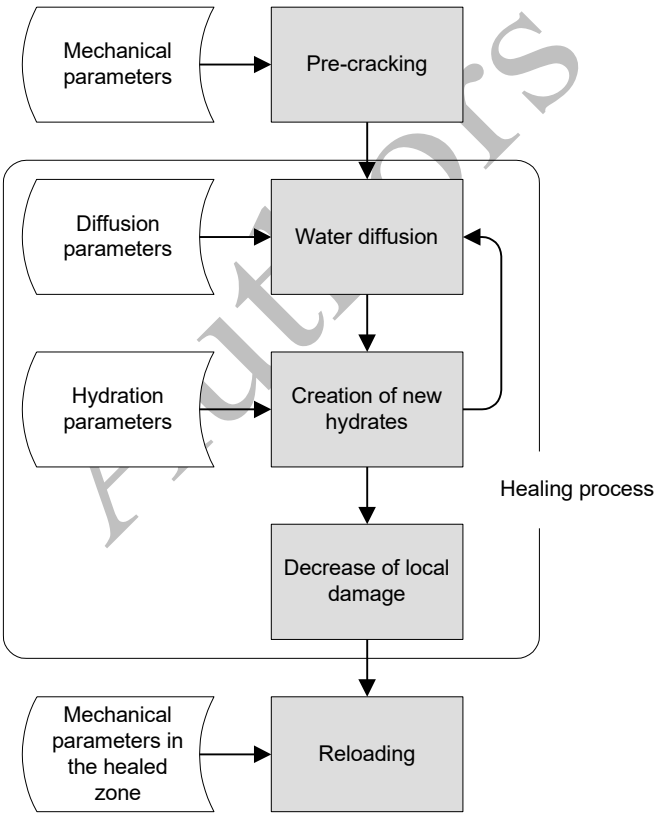

449

450 **Figure 2.** Flowchart of the model to study the impact of self-healing on mechanical

451 properties

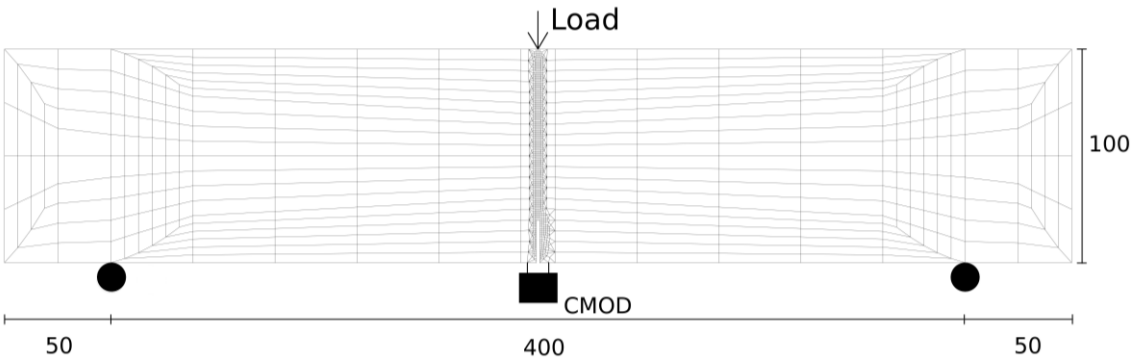

452

453 **Figure 3.** Notched beam: geometry, mesh, position of numerical CMOD and loading

454

455

456

457

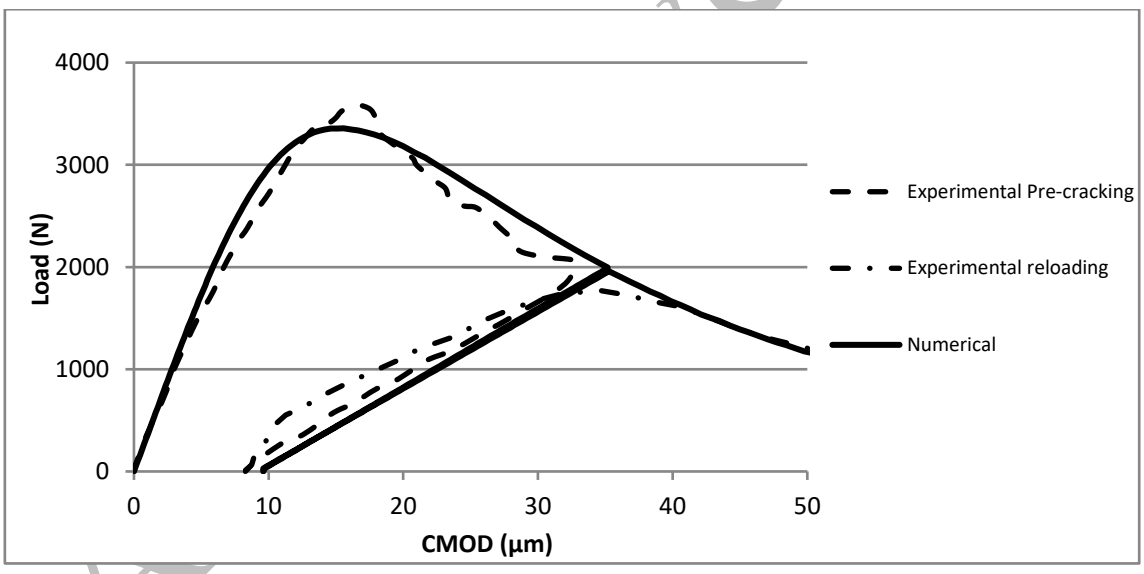

458

459 **Figure 4.** Numerical loading curve of the virgin specimen compared to mean

460 experimental data from [14, 34].

461

462

463

464

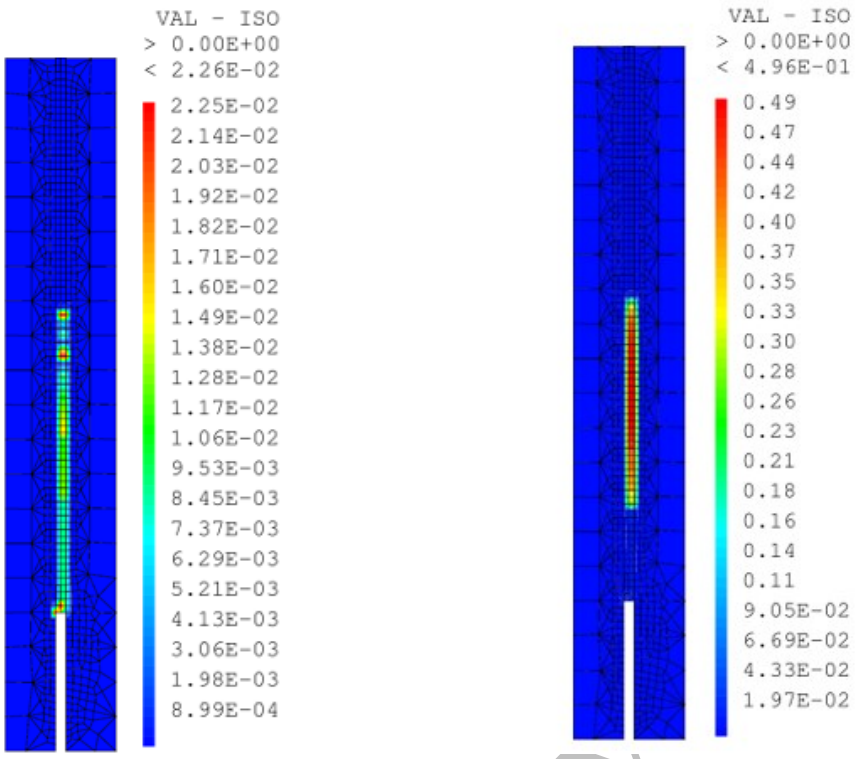

a) b)

Figure 5. Residual damage after 20 days of healing a) with normal diffusion and hydration parameters (residual damage close to 0 all along the crack), b) with increased hydration (crack completely healed at its bottom part)

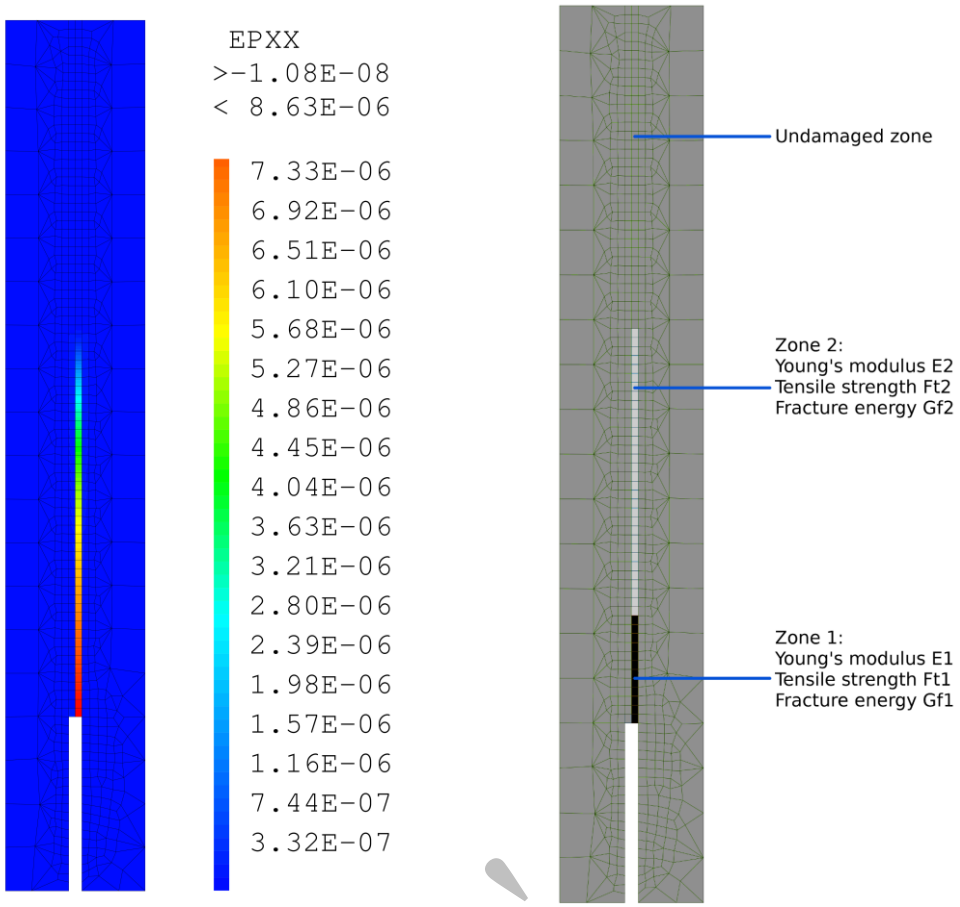

a) b)

Figure 6. Initial numerical crack width (in meter) (a) and two-phase healing model (b)

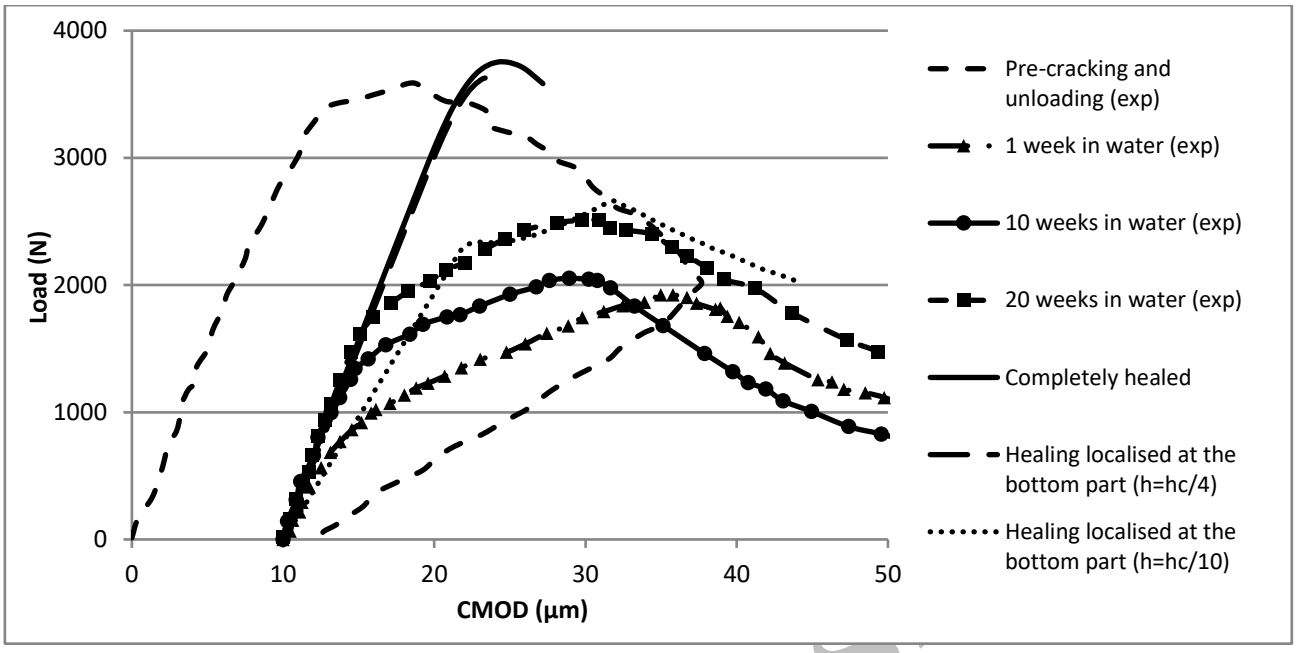

471

472 **Figure 7.** Influence of the extend of the healed zone during reloading on numerical curves

473 compared to experimental curves (h is the height of the healed zone, hc the height of the

474 crack)

475

476

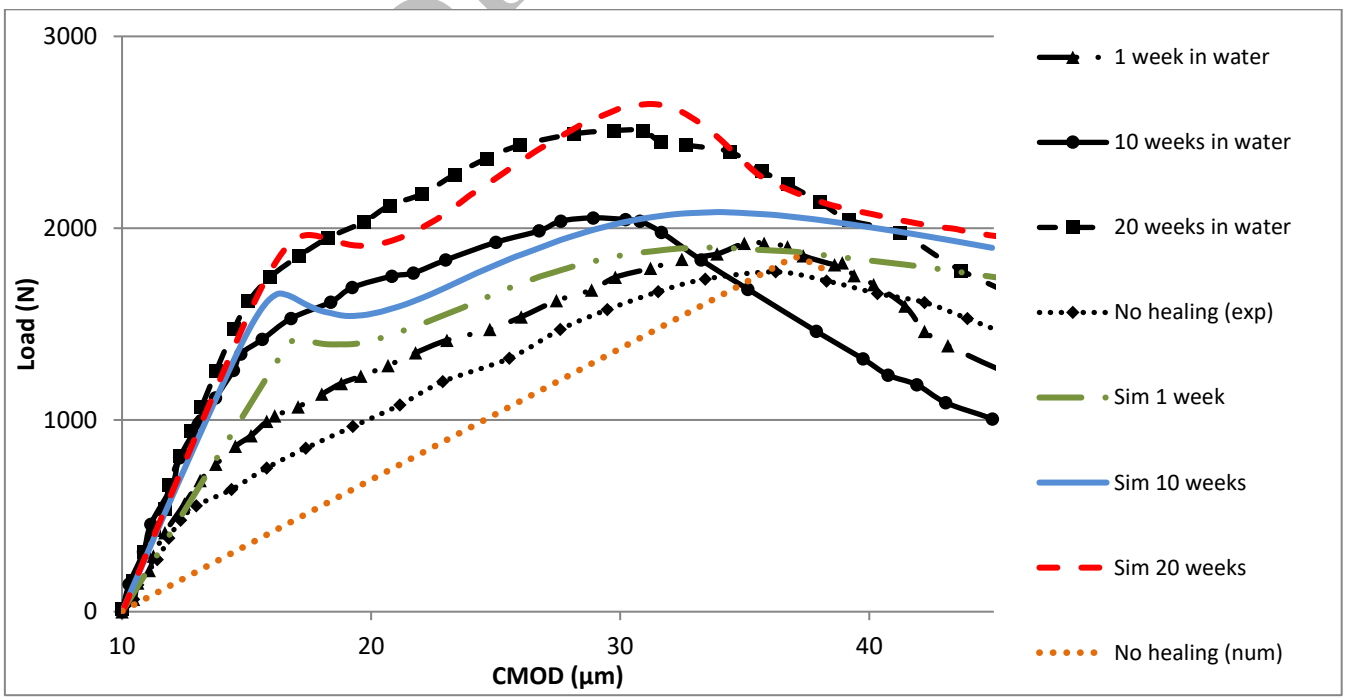

477

478

479 **Figure 8.** Experimental and numerical reloading curves for different healing periods